Controlled Engineering of WS_2 Nanosheets-CdS Nanoparticle Heterojunction with Enhanced Photoelectrochemical Activity

M. Zirak[1], M. Zhao[2], O. Moradlou[3], M. Samadi[1], N. Sarikhani[4], Q. Wang[2], H. –L. Zhang[2]*, A. Z. Moshfegh[1,5*]

[1]*Department of Physics, Sharif University of Technology, P.O. Box 11555-9161, Tehran, Iran*

[2]*State Key Laboratory of Applied Organic Chemistry, College of Chemistry and Chemical Engineering, Lanzhou University, P.O. Box 730000, Lanzhou, P. R. China*

[3]*Department of Chemistry, Alzahra University, P.O. Box: 1993893973, Tehran, Iran*

[4]*Department of Mechanical Engineering, Sharif University of Technology, P.O. Box 11555-9567, Tehran, Iran*

[5]*Institute of Nanoscience and Nanotechnology, Sharif University of Technology, P.O. Box 14588-8969, Tehran, Iran*

* *Corresponding authors'* Email: AZM: moshfegh@sharif.edu, HLZ: Haoli.zhang@lzu.edu.cn

Abstract

We report the well-controlled preparation of WS_2 nanosheets-CdS nanoparticle heterojunction potentially applicable for photoelectrochemical (PEC) water splitting under visible light. The WS_2-few layers nanosheets with an average thickness of ~5 nm and lateral dimensions of ~200 nm were synthesized via a convenient liquid phase exfoliation of bulk WS_2 in water/ethanol solution, which can be readily deposited onto ITO substrate via electrophoretic deposition. CdS nanoparticle thin films were synthesized via facile successive ion layer absorption and reaction (SILAR) method. By combining these two simple and well-controlled methods, CdS/WS_2/ITO and WS_2/CdS/ITO thin films were fabricated. The loadings of WS_2 nanosheets and CdS nanoparticles were carefully controlled by the deposition condition and the heterojunction was

optimized for enhanced photoelectrochemical response under simulated sunlight irradiation. The obtained heterojunction structures were characterized by various techniques, including scanning electron microscopy (SEM), PEC response and electrochemical impedance spectroscopy (EIS). Our results showed that the CdS/WS_2/ITO heterojunction can exhibit a very stable photo-current density 3 times higher than the conventional CdS/ITO thin films under the same conditions. In contrast, photo-current density of the WS_2/CdS/ITO thin films was lower than that of the bare CdS/ITO, indicating that an appropriate energy level cascade is essential for achieving enhanced PEC response. A charge transfer mechanism was proposed to explain the observed PEC enhancement. This work indicates that the liquid phase exfoliated WS_2 nanosheet is a promising new material for photoelectrochemical applications and our applied method is very simple but effective to deposit CdS and WS_2 nanostructures to give stable performance under long time light irradiation.

Keywords: WS_2-CdS heterojunction, well-controlled growth, photoelectrochemical performance, visible light, charge transfer mechanism

1. Introduction

Recently, there has been considerable interest in the study of the two-dimensional (2D) layered materials such as graphene and transition-metal dichalcogenides (TMDs). TMDs as graphene analogues are a family of compounds with the formula of MX_2, where M is a transition metal element and X is a chalcogen (S, Se or Te). The covalently bonded 2D X-M-X layers are separated by weak Van der Waals interactions, which can be exfoliated into

single-layer or few-layers via various methods. Several 2D TMD materials have exhibited attractive properties including high mobility, large surface area, structure-dependent band structure and high catalytic activity.

It is known that the electronic properties of 2D TMD materials are strongly dependent on their morphology and preparation method. For instance, WS_2 is an indirect band gap material in its bulk form (1.35 eV) and becomes a direct band semiconductor with a gap of 2.05 eV in the mono-layer form, which exhibits extraordinary electrical and optical properties. Besides, 2D-WS_2 layers prepared by lithium intercalation and exfoliation show metallic properties, while that prepared by solvent exfoliation method exhibit semiconductor properties.

It is well established that 2D layered composite materials possess larger specific surface areas that lead to a large number of active sites on their surface, which can significantly enhance the catalytic activity. Based on the recent reports, among the TMDs family, exfoliated MoS_2 and WS_2 are less toxic compared to graphene oxide and therefore, they can be employed as a safer alternative in future applications. WS_2 has a higher intrinsic electrical conductivity than MoS_2, and therefore is a more suitable candidate for fabrication of hybrid composite. Layered hybrid composites of the WS_2, including WS_2/CN, WS_2/rGO and ZnS–WS_2/CdS with enhanced hydrogen production activity were reported.

Few layers of WS_2 with the large surface area, high active sites and broadband light absorption is predicted to enhance the CdS photo-activity. Chen et al. reported the co-loading of ZnS and WS_2 on CdS particles to produce ZnS-WS_2/CdS powders and demonstrated that the loading increased the photocatalytic activity of CdS particles significantly. But the used preparation method was time and energy consuming.

To the best of our knowledge, there is no report about preparation of WS_2-CdS thin film electrode and investigation of its PEC performance. Herein, we have introduced a very simple

combined method to prepare the CdS-WS_2 heterojunction thin film electrodes with stable PEC performance for the first time. We have fabricated the WS_2/CdS hybrid films, composing 2D WS_2 nanosheets and CdS nanoparticles using a facile and safe deposition method at room-temperature . Herein, CdS/WS_2/ITO and WS_2/CdS/ITO thin film electrodes with various amounts of CdS and WS_2 nanosheet loading were prepared by simple and well-controlled successive ion layer adsorption and reaction (SILAR) and electrophoretic deposition (EPD) methods. Different properties of the hybrid thin films, including their photoelectrochemical performance, were carefully studied, using various analytical techniques. The charge transfer mechanism in the CdS-WS_2 interface of the both CdS/WS_2/ITO and WS_2/CdS/ITO thin films is proposed to account for the observed PEC behavior. Our simple applied method was very effective to deposit CdS nanoparticles and WS_2 nanosheets with excellent cohesion to the substrate which results in robust photoresponsibility under continuous long time light irradiation.

2. Experimental

Preparation of exfoliated WS_2 few layers

Based on our previous study, exfoliated WS_2 few layer nanosheets were obtained via mixed-solvent strategy. Typically, 500 mg bulk WS_2 powder was dispersed in 100 mL flask containing 50 mL mixed water/ethanol solution (with the volume fraction of water:ethanol=65:35). The flask was capped tightly and put in the sonication bath and then sonicated for 15 h. After 48 h rest in the room condition, the 2/3rd of the supernatant was selected and centrifuged at 3800 rpm for 45 min and finally, the upper 2/3rd of the centrifuged solution was decanted into glass vials and kept for further use.

Preparation of WS_2 few layers thin films

Electrophoretic deposition (EPD) was utilized to prepare WS_2 exfoliated few-layers thin films. Before deposition, the ITO sheets were cleaned as following: they were washed by dish soap carefully and then sonicated for 30 min in DI water. The procedure was repeated again. After that the ITO sheets were sonicated in Acetone for 30 min and sonication in Acetone was also repeated again. Finally the ITO sheets were sonicated in Isopropyl alcohol 2 times and each time for 30 min.

Two pre-cleaned ITO sheets were chosen as an anode and cathode, respectively, and placed at the distance of 15mm from each other in a parallel alignment. The WS_2 suspension in water:ethanol was the electrolyte. Based on zeta potential measurement studies, WS_2 flakes carry electrical charges in water:ethanol solution. So, there is no need to add a conductive electrolyte. By applying 8V between these two electrodes for different time intervals (30 s, 1 and 2 min), the WS_2 thin films were deposited on the ITO cathode. Since, the EPD lower than 30s resulted in no significant WS_2 deposition, 30s was selected as a minimum required deposition time.

CdS nanoparticles deposition

Based on our previous works, the successive ion layer adsorption and reaction (SILAR) method was employed for CdS nanoparticles loading. The ITO or WS_2/ITO electrodes were separately immersed into 50 mM $Cd(NO_3)_2$, and then 50 mM Na_2S aqueous solutions for 20 s. The layers were rinsed with deionized (DI) water after each immersion step. This sequential process (known as SILAR cycle) was repeated 20 times. To prepare WS_2/CdS/ITO thin films, CdS were being loaded via SILAR technique and then WS_2 was deposited on CdS/ITO thin film by EPD method. In order to fabricate CdS/WS_2/ITO films, as the first step, WS_2 was deposited

on ITO via EPD, and then CdS nanoparticles were deposited on the prepared WS_2/ITO thin film using SILAR method.

Material characterization

UV-Visible absorption spectra of the samples were obtained via PGENERAL T6 spectrophotometer. To investigate the topographical properties and morphology of the prepared thin films, tapping-mode atomic force microscopy, AFM (Agilent SPM 5500, USA) and field-emission scanning electron miceroscopy (FE-SEM) (Hitachi S4800) were employed. The AFM data were analyzed with SPIP 6.2.8 software. High resolution transmission electron microscopy, HRTEM (Tecnai-G2-F30, USA) equipped with X-ray energy dispersive spectrometer, EDS (Oxford Link-ISIS) was used to study the morphology chemical composition of the nanostructures. The Invia Renishaw Raman microscope was also employed to identify the composition of the samples. The exciting laser wavelength was 514.5 nm and the Raman spectra were calibrated using Si Raman peak at 520 cm^{-1} as reference.

3. Results and Discussion

Various properties and performance of the prepared samples were investigated using the above analytical techniques. In this section, we report the results of optical study, AFM analysis, Raman spectroscopy, TEM observations, Photoelectrochemical activity as well as a proposed mechanism for the photo-enhancement of water splitting under visible light as follows:

Optical Analysis

The layered structure of 2H-WS_2 is shown in **Fig. 1** inset. The thickness of a single-layer WS_2 is 6.162 Å. Each layer consists of an atomic plane of hexagonally- arranged W atoms sandwiched between two similar hexagonally- arranged atomic S planes. The bond within the

layers is covalent while these layers are bonded together by weak van der Waals forces in AbA|BaB stacking order in 3D crystal. This 2H crystal structure of WS_2 has a specific UV-visible absorption spectrum. So, it can be a good criterion to understand if the prepared WS_2 solution has a 2H crystal structure or not.

The optical spectrum of the WS_2 few layer solutions (after scattering subtraction) is shown in **Fig.** 1. Excitonic A and B absorption peaks appeared at about 628 and 525 nm, respectively. These two peaks are arising from direct gap transitions at the K point of the 2H-WS_2 unit cell. The weak absorption peak C appeared at ~ 455 nm is related to the optical transitions between the density of states in the valence band (VB) and conduction band (CB).

Fig. 1

The relationship of $(\alpha h\nu)^n=A(h\nu- E_g)$ is used to calculate the energy band gap (E_g) of the direct band gap semiconductors (n=2) and indirect band gap semiconductors (n=1/2). These plots for various WS_2/CdS/ITO and CdS/WS_2/ITO thin films are shown in **Figure 2a** and **Figure 2b**, respectively. The insets are the corresponding absorption spectra. Evaluated energy band gaps of the samples are presented in **Table 1**. For all of the samples, the increase in the EPD time (which resulted in an increase in WS_2 loading) cause a shift in the E_g from 2.5 eV (in bare CdS) to 1.7 eV for bare WS_2 (Figure S1, Supporting Information).

Table 1

The E_g values were decreased from 2.5 to 1.7 eV for the WS_2/CdS/ITO samples, but for the CdS/WS_2/ITO thin film samples, the E_g values were reduced to 2.1 eV, which indicates that in the latter system, the CdS crystal plays an important role for light harvesting.

Figure 2

AFM Observations

The AFM analysis was employed to reveal both thickness and lateral dimension of the exfoliated nanosheets. WS_2 solution was spin-coated on a mica substrate at 2000 rpm for 20 s. The results are shown in **Figure 3**. As it can be seen, there are a distribution of flakes with thickness between 1-5 nm and lateral dimensions varied between 50 - 350 nm. The average thickness and lateral dimension of the WS_2 flakes were measured to be about 5 nm and 200 nm, respectively. The thickness of a monolayer MoS_2 and WS_2 prepared via chemical methods was reported to be about 0.8–1.2 nm. Hence, the obtained flakes are estimated to be 5 layers in average. The observed thickness below 1 nm in **Figure 3e** is as a result of AFM technique. Tapping mode was used to get AFM images. The real thickness and size should be determined after subtraction of these effects of AFM instrument. It is worth to note that thses flakes (with above mentioned thickness and sizes) make clusters with different thickness and sizes after deposition on ITO substrate with various deposition time which can affect the PEC performance of the layers. the effect of various deposition time on PEC performance is carefully discussed in following sections.

Figure 3

Raman characterization

The bulk 2H-WS_2 belongs to the space-group ($P6_3/mmc$, #194), with unit cell consisting of two W atoms lie in (2d) Wyckoff position ±(1/3,2/3,3/4) and four S atoms in (4f) Wyckoff position ±(1/3,2/3,1/4±z) with z=0.1225≈1/8. The 2H notation stands for Hexagonal form with 2 molecular units in the primitive unit cell to distinguish from the other Rhombohedral polytype, 3R, with 3 molecular units in the unit cell, (**Figures S2a** and **S2b**). Details of crystal structure,

Raman active modes of WS_2 layers and their corresponding atomic displacements are illustrated in **Figure S2c**.

To ensure that both CdS and WS_2 are successfully deposited together onto ITO substrate, the final thin films were subjected to Raman spectroscopy. The exciting laser wavelength was 514.5 nm (Ar laser) in the back scattering geometry. To assess the possibility of oxidation during Electrophoretic Deposition (EPD), the Raman spectra of the samples prepared with longest EPD time (2 min) were examined and the results are shown in **Figure 4**. Two obvious Raman peaks located at 355.0 and 419.6 cm^{-1} are attributed to E^1_{2g} and A_{1g} first-order optical modes of WS_2, respectively. The separation between the two modes is 64.6 cm^{-1}, lies between 64.8 cm^{-1} for bulk WS_2 and 62 cm^{-1} for monolayer formation, which indicates the presence of few-layer WS_2.

The thickness of WS_2 flakes would affect the positions of the peaks in Raman spectra as well as their intensities. In particular, the peak position of out-of-plane mode, A_{1g}, has a strong dependency to the number of layers in WS_2 flakes and can be quantified to estimate the average number of layers using an exponential model $\omega_{A_{1g}}(N) = \omega_{bulk} + (\omega_{1L} - \omega_{bulk}) Exp\left[-\chi(N-1)\right]$ and a fractional model $\omega_{A_{1g}}(N) = \omega_{bulk} + (\omega_{1L} - \omega_{bulk}) / \left[1 + \chi(N-1)\right]$ where N is the number of layers, χ the fitting parameter and $\omega_{A_{1g}}$, $\omega_{bulk} = 420.1$ and $\omega_{1L} = 417.2$ are measured, bulk and mono-layer A_{1g} peak position of WS_2 in cm^{-1}, respectively. By fitting these two models and based on the reported data for various WS_2 thickness in literatures, we have obtained $\chi = 0.495$ for exponential model and $\chi = 0.796$ for fractional model using Raman spectroscopy at exciting laser wavelength of 514.5 nm. However, the mean absolute deviation (MAD) as a criterion for the fitting goodness is better for the exponential model than the fractional model. Thus, by using

the exponential model, the average number of layers for $\omega_{A_{1g}}(N) = 419.6\ cm^{-1}$ in **Figure 4** is estimated to be $N \approx 5$ layers, which confirms the AFM observations.

The two characteristic CdS longitudinal optical (LO) phonon mode peaks can be seen at about 300 cm^{-1} (1LO) and 600 cm^{-1} (2LO). The line shape asymmetry and the shift of the peak toward lower frequencies compared to the bulk CdS (305 cm^{-1} and 605 cm^{-1}) can be attributed to optical phonon confinement and formation of CdS nanoparticles. Figure 4 clearly verifies the presence of both CdS nanoparticles and WS_2 few layers in both WS_2/CdS/ITO and CdS/WS_2/ITO thin films without any trace of oxides.

Figure 4

TEM Analysis

To further study and verify successful junction formation between the CdS particles and WS_2 sheets, TEM analysis was also employed. The CdS-WS_2 materials were crashed from the CdS/WS_2/ITO (8V-30s) sample with a keen blade and then dispersed in water and exposed to vigorous sonication for 1h.

TEM results are shown in **Figure 5**.

As it can be seen, the CdS particles are blended into WS_2 sheets. Higher magnification of the selected area (**Figure 5b and c**) shows clearly the presence of both WS_2 sheet and CdS planes (220). The hexagonal structure of WS_2 sheet can be seen obviously in **Figure 5c**, indicating that no crystal structural change occurred during our preparation method, which is in good agreement with the obtained optical absorption spectrum and Raman analysis. The EDS spectrum and atomic percentage of the elements are shown in **Figure 5d**.

Figure 5

Photoelectrochemical Measurements

Chronoamperometry

J-t curves of the CdS/WS_2/ITO and WS_2/CdS/ITO samples are shown in **Figure 6** and **Figure 7** and the results are compared to the bare CdS/ITO thin films, respectively. Photo-current density measured for the CdS/ITO thin films was about 125 μA/cm^2. All of the CdS/WS_2/ITO thin films have higher photo-activity than the bare CdS thin film, while, the bare CdS thin film exhibits a higher photo-activity than the WS_2/CdS/ITO samples. Photo-current density of 350, 290 and 274 μA/cm^2 is measured for the CdS/WS_2/ITO thin films prepared with 30s, 1 and 2 min deposition time by EPD method, respectively.

The order of photoactivity of the prepared samples is as following:

CdS/WS_2/ITO > CdS/ITO > WS_2/CdS/ITO

So, if the ITO substrate is covered with few layers of WS_2 before deposition of CdS nanoparticles, the photo responsivity of the system can be improved to about 3 times.

The charge transfer condition is different in CdS/WS_2/ITO and WS_2/CdS/ITO thin film systems. The photoresponsivity of bare WS_2/ITO thin films prepared with various EPD time is also measured and the results are shown in **Figure S3**, indicating low photoactivity of WS_2/ITO thin films compared with WS_2-CdS/ITO thin films.

Figure 6, Figure 7

The effective surface area of samples plays a decisive role in both light absorption and catalytic reactions as reported by others. Thus, the surface areas of the prepared thin films were compared through their surface roughness (S_r) measured via AFM technique. The different regions of the surface were examined in a statistical manner.

The results are summarized in **Table 1**.

In CdS/WS_2/ITO thin films the WS_2 flakes are deposited on conductive ITO substrate. In this situation, the induced E is strong and WS_2 flakes are deposited more quickly. Therefore the highest surface roughness is obtained by short deposition time (30 s) and after that the roughness decrease and reaches to a saturated value (table 1). In the other hand, for WS_2/CdS/ITO thin films, the WS_2 flakes are deposited on CdS/ITO substrate. Deposition of semiconducting layer of CdS on ITO decrease the net electrical filed. The roughness of WS_2/CdS/ITO thin films increase by increasing deposition time. It is expected that their S_r reach to a maximum value and then to a saturated one in deposition times longer than 2 min. because the PEC performance of these samples decrease with increase in EPD time, it is not reasonable to prepare the samples with deposition time longer than 2 min. The S_r value for the CdS/WS_2/ITO thin films is also higher than that of the bare CdS layer. The highest S_r is obtained for the sample grown under 30s deposition of the WS_2 few layers (**Table 1**). This result agrees well with the highest photo-current density measured for this sample. Therefore, in these systems, the higher S_r is in favor of photo-current enhancement. The 2D-AFM images representing the surface topography of various synthesized samples are shown in Figure S4.

The photo-current density as a function of light intensity spectra and also their logarthmic spectra, to obtain the scaling exponent, for the CdS/WS_2/ITO and the WS_2/CdS/

ITO thin films are shown in **Figure S5** and **Figure S6**, respectively, which are in good agreement with corresponding J-t curves (**Figure 6** and **Figure 7**).

The photo-current density of the bare CdS/ITO is less than CdS/WS_2/ITO and higher than WS_2/CdS/ ITO thin films in all of various light intensities (CdS/WS_2/ITO>CdS>WS_2/CdS/ITO). The β exponents for these systems are evaluated and listed in **Table 1**. The obtained β for CdS/WS_2/ITO is greater than bare CdS, indicating favorable situation for charge transfer in these samples compared to CdS thin films. The greatest β value is related to CdS/WS_2/ITO prepared with 30 s EPD which has also the highest photo-responsibility. Further deviation from linear behavior by increasing EPD time indicates that both the layers charge transfer resistance and their saturated effect are increasing and this can be signs of bimolecular recombination.

It was found that all of the WS_2/CdS/ ITO thin films have smaller β values, meaning that the conversion of light to current is less efficient in these samples and loading of WS_2 nanosheets on the CdS/ITO thin film is not in favor of charge separation and transportation. **Figure 7** and **Table 1** show that higher WS_2 loading in these samples resulted in lower photo-current density and also smaller β value. WS_2 deposition in the WS_2/CdS/ ITO thin films increased the surface area and as a result the light absorption was enhanced (**Figure 2** and **Table 1**), which however cannot generate higher current density in an efficient manner. The obtained value of β= 0.68 for the WS_2/CdS/ ITO (8V- 2 min) sample is the minimum and the nearest value to β_{free}, indicating that bimolecular recombination is the most dominant effect in this configuration.

Electrochemical Impedance Spectroscopy

Nyquist plots of the bare CdS/ITO, CdS/WS_2/ITO(8V -30s) and WS_2/CdS/ITO(8V –30s) thin films are shown and compared in **Figure 8**. Semicircle of the CdS/WS_2/ITO(8V-30s) thin film is smaller than that of the bare CdS/ITO thin film indicating lower charge transfer resistance in the

CdS/WS_2/ITO thin film. The data can be fitted with a Randles circuit (**Figure 8** inset) which is reported for similar systems elsewhere. The charge transfer resistances (R_{ct}) for the samples are listed in **Table 1**. R_{ct} for bare CdS/ITO thin film is 2365 Ω which is larger than 2088 Ω for CdS/WS_2/ITO (8V –30s) thin film and smaller than 6755 Ω for WS_2/CdS/ITO (8V–30s) layer.

Figure 8

Nyquist plots of the CdS/WS_2/ITO layers are shown in **Figure S7**. Increase in EPD time resulted in an increase in charge transfer resistance (**Table 1**) leading to reduction of the photo-current density of the samples. On the other hand, Nyquist plots of other WS_2/CdS/ITO systems show a higher R_{ct} as compared to the bare CdS thin film (**Figure S8**).

Stability of the photoelectrodes

One of mos important properties of a photoelectrode in solar driven water splitting and solar cell application is its stability under continoius sunlight irradiation for a long time. The stability of the CdS/WS_2/ITO (8V-30s) which has given the best photo-current density was investigated under continuous irradiation of our Xe lamp for 90 min and compared with bare CdS/ITO electrode. The results are shown in Figure 9. Low stability of CdS thin films because of photo-corrosion effect is a well known fact which is clear in Figure 9. But the CdS/WS_2/ITO (8V-30s) sample gives a stable phto-current with nearly no decrese after 90 min continius light irradiation. The results indicate that charge carrier separation and transport is more dominant than CdS photo-corrosion in CdS-WS_2 heterojunction. Adding appropriate amount of few-layer WS_2 to highly photo-active CdS thin film, increase its phto-activity and also its stability which both of these factors are very important issues in solar energy material fabrication. The results indicate that our applied method was very simple but effective to prepare CdS-WS_2 heterojunction thin

film with excellent cohesion to the substrate which results in robust photoresponsibility under continuous long time light irradiation.

Figure 9

Mechanism of photo-enhanced PEC property

Investigation and comparison of the WS_2/CdS/ITO and CdS/WS_2/ITO thin film systems with different photoelectrochemical behavior provide obvious evidence to understand the charge transfer mechanism in CdS-WS_2 heterojunction. By contrast, this good electron pathway should be blocked in the WS_2/CdS/ ITO thin film, resulting in lower photo-current density. The schematic representation of charge transport processes in these two thin film systems are illustrated in **Figure 10**. Thses issues are verified by SEM observation (**Figure S8**). Uniform coating of both CdS and WS_2 layer on ITO substrate can be clearly observed in Figure S8b and Figure S8c, respectivly. Upon visible sunlight irradiation, both CdS and WS_2 can be excited to generate e^--h^+ pairs. This suitable condition is observed only for the CdS/WS_2/ITO thin films. As shown in **Figure 10a**, for the CdS/WS_2/ITO system, the appropriate position of conduction band (CB) alignment, the photo-generated electrons can be transferred stepwise from CB of CdS to CB of WS_2 and then to ITO substrate. Meanwhile, photo-generated holes can also transfer stepwise from the CdS valence band (VB) to WS_2 nanosheets VB and accumulate for the subsequent oxidation process. This efficient electron-hole separation and transport is the key factor to protect the CdS layer against photo-corrosion, resulting in generation of a sustainable photo-current (**Figure 9**). If the excess CdS loading is covering most areas of the WS_2 nanosheets it may prevent the transfer of holes to the solution and as a result, their recombination process may occur, leading to reduction of photo-current density of the sample. Based on Table 1, the optimum condition for the CdS/WS_2/ITO thin film is 30 s EPD time.

The impedance spectroscopy results indicate that the CdS/WS_2/ITO (8V-30s) system has the lowest charge transfer resistance as compared with other samples prepared with higher EPD time. Because of the anisotropic conductivity of WS_2, a higher resistance is detected when the amount of the WS_2 layers increase, also supported by our EIS results (See **Figure 8**). So it is logical that higher EPD deposition time increases the WS_2 layer thickness resulting in deterioration of the photocurrent density. Accordingly, increase in EPD time results in increase in deposited WS_2 flakes, less surface roughness and higher charge transfer resistance (**Table 1**).

For the WS_2/CdS/ ITO thin film system, we have also found the appropriate conditions for hole transport process. The pathway for hole migration is the same as in the CdS/WS_2/ITO thin films. As a result, these electrons accumulate in CB of WS_2 and recombine with the generated holes in the VB of WS_2. This proposed mechanism is also verified by impedance results (Figure S7). Based on our data analysis and the results in Table 1, the WS_2/CdS/ITO thin films prepared by longer EPD deposition have a higher surface area and as a result, they have more surface sites for reactions. But, due to blockage of electron pathways toward back contact, increasing surface sites resulted in increasing recombination centers leading to a drastic reduction of photo-activity of the sample.

Figure 10

Conclusions

WS_2 few layer nanosheets were prepared through solvent exfoliation in a mixed water/ethanol solution without using any additives. The obtained WS_2 flakes were combined with CdS nanoparticles to produce WS_2/CdS/ITO and CdS/WS_2/ITO thin films electrodes via simple electrophoretic and SILAR methods. Taking advantages of this combined method, loading of both CdS nanoparticles and WS_2 few layers can be well controlled and various architectures

were easily designed and produced. In this approach, CdS-WS_2 heterojunction was fabricated and its photoelectrochemical (PEC) activity was investigated systematically under sunlight irradiation. The PEC results indicate that in the CdS/WS_2/ITO thin film system, there is an appropriate pathway for photo-generated charge carriers and synergistic effect of CdS and WS_2 material resulted in a much higher photo-current density as compared to individual components and also protect them against phto-corrosion and therefore a stable phto-current can be achieved. However, in the WS_2/CdS/ITO thin film system, the photo-generated electrons in the CB of WS_2 flakes cannot transfer to back contact through the CdS nanoparticle mediator. Thus, these trapped electrons may recombine with the accumulated holes in VB of WS_2 nanosheets. As a result, the photo-current density of the WS_2/CdS/ITO thin films is reduced as compared with the bare CdS thin film. The obtained results for the WS_2/CdS/ITO and the CdS/WS_2/ITO thin films support our charge transfer mechanism in the CdS-WS_2 heterojunction. The results herein can provide useful information for future device applications of these materials.

Appendix A. Supporting information

Electronic Supplementary Information (ESI) is available in a separate file.

Fig. 1

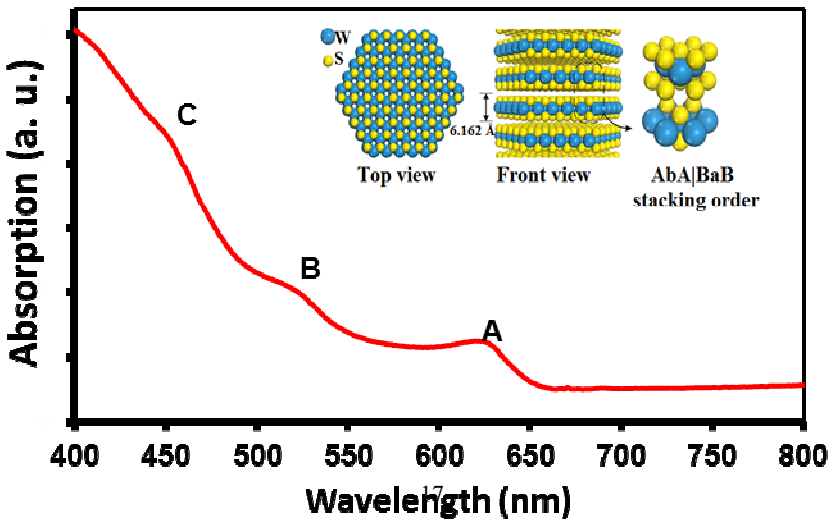

Fig. 2

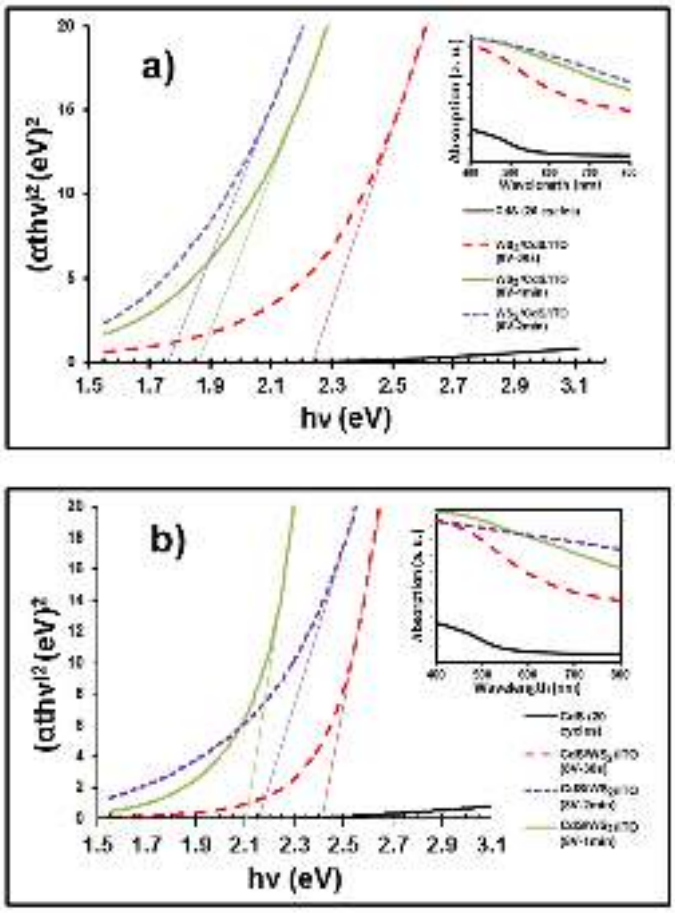

Fig. 3

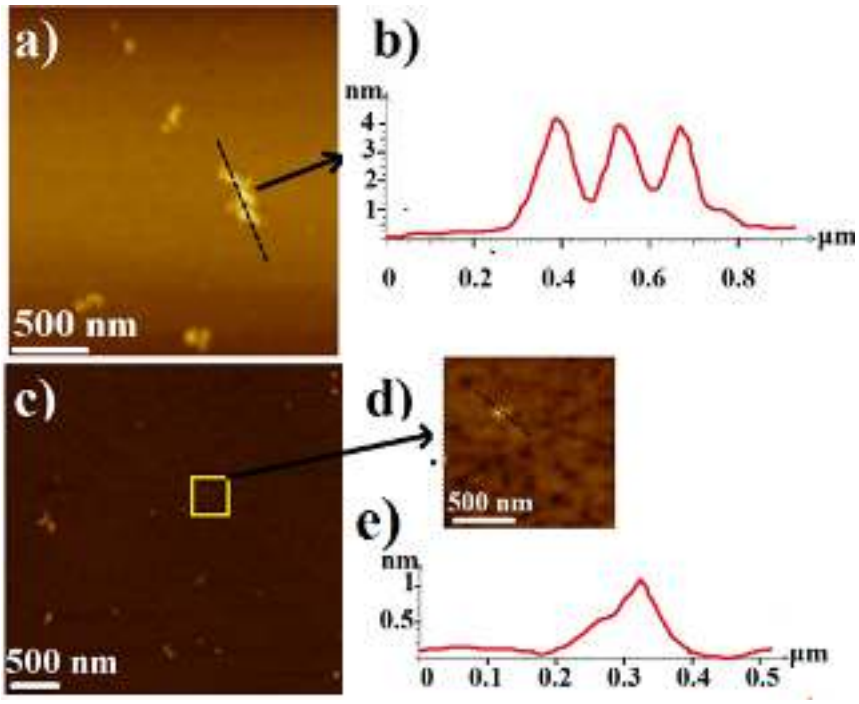
a)
500 nm
b)
nm
4
3
2
1
0
0.2
0.4
0.6
0.8
μm
c)
500 nm
d)
500 nm
e)
nm
1
0.5
0
0.1
0.2
0.3
0.4
0.5
μm

Fig. 4

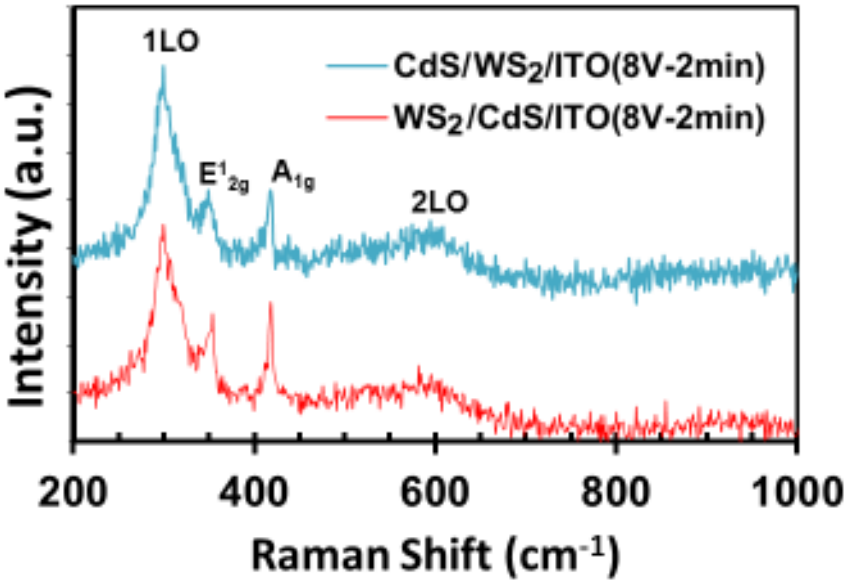
1LO
CdS/WS2/ITO(8V-2min)
WS2/CdS/ITO(8V-2min)
E12g
A1g
2LO
Intensity (a.u.)
200
400
600
800
1000
Raman Shift (cm-1)

Fig. 5

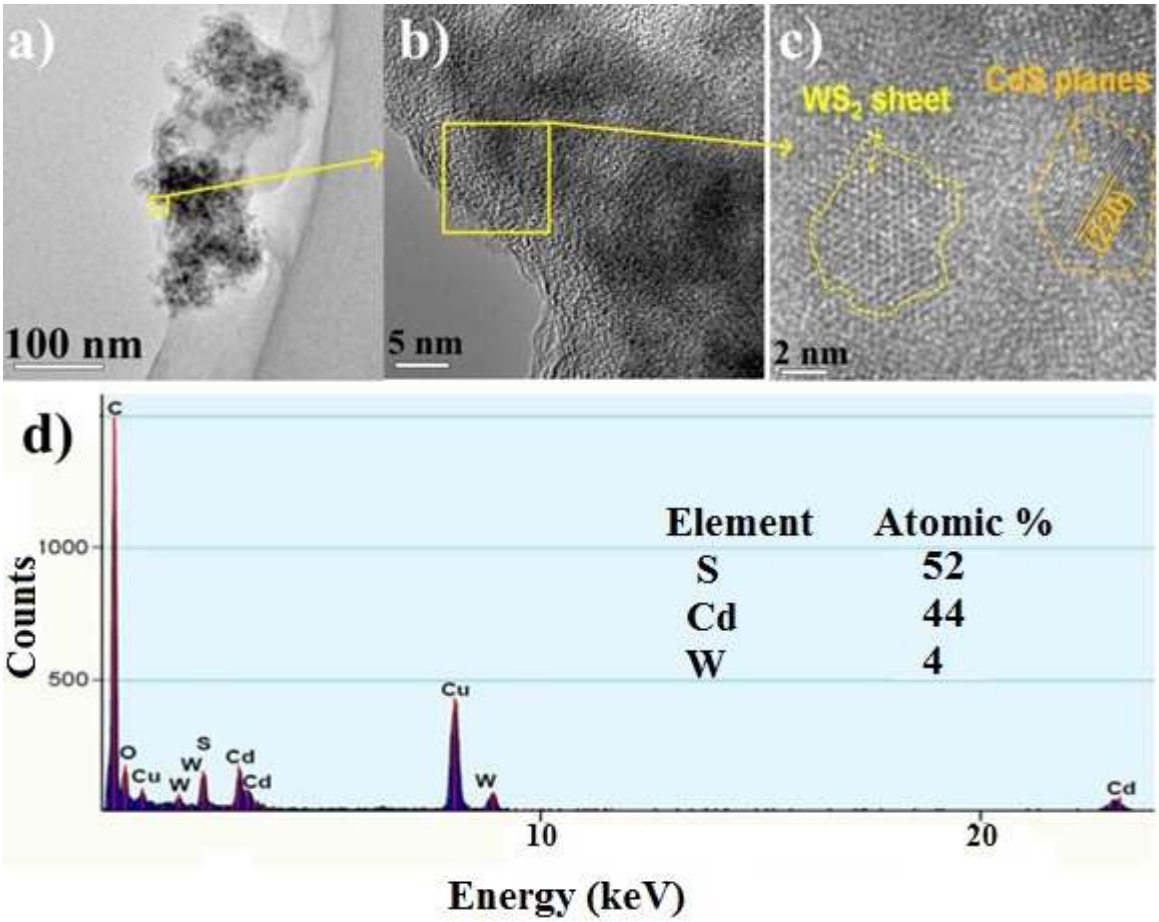
a)
100 nm
b)
5 nm
c)
WS2 sheet
CdS planes
2 nm
d)
Element Atomic %
S 52
Cd 44
W 4
Counts
1000
500
C
O
Cu
W
W
S
Cd
Cd
Cu
W
Cd
10
20
Energy (keV)

Fig. 6

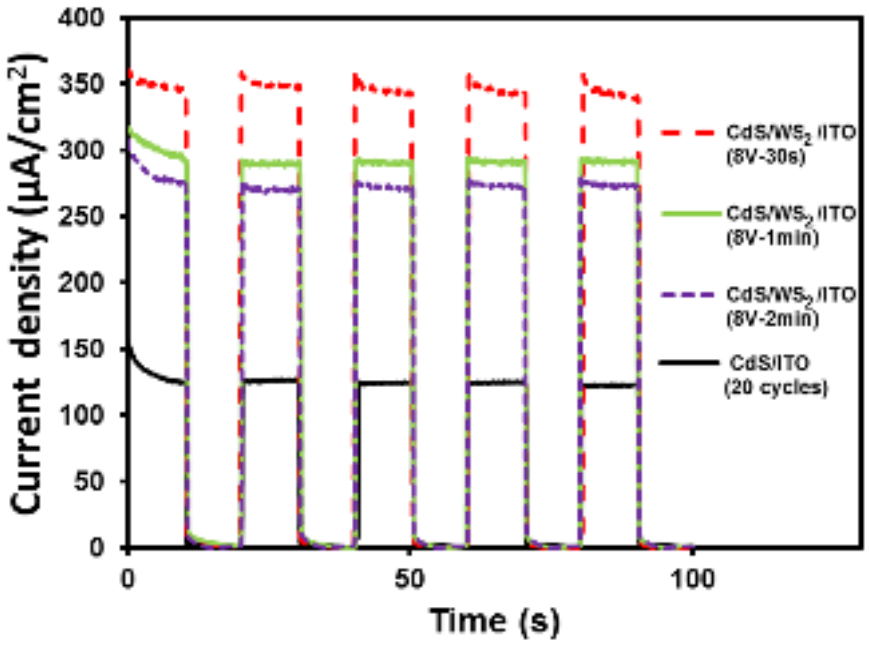
Current density (μA/cm²)
Time (s)
CdS/WS2 /ITO (8V-30s)
CdS/WS2 /ITO (8V-1min)
CdS/WS2 /ITO (8V-2min)
CdS/ITO (20 cycles)

Fig. 7

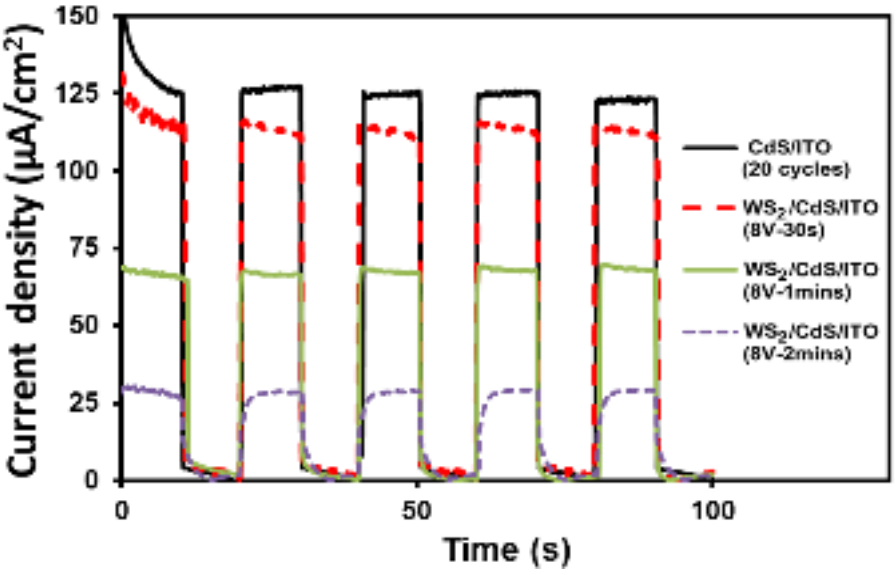
Current density (μA/cm²)
Time (s)
CdS/ITO (20 cycles)
WS2/CdS/ITO (8V-30s)
WS2/CdS/ITO (8V-1mins)
WS2/CdS/ITO (8V-2mins)

Fig. 8

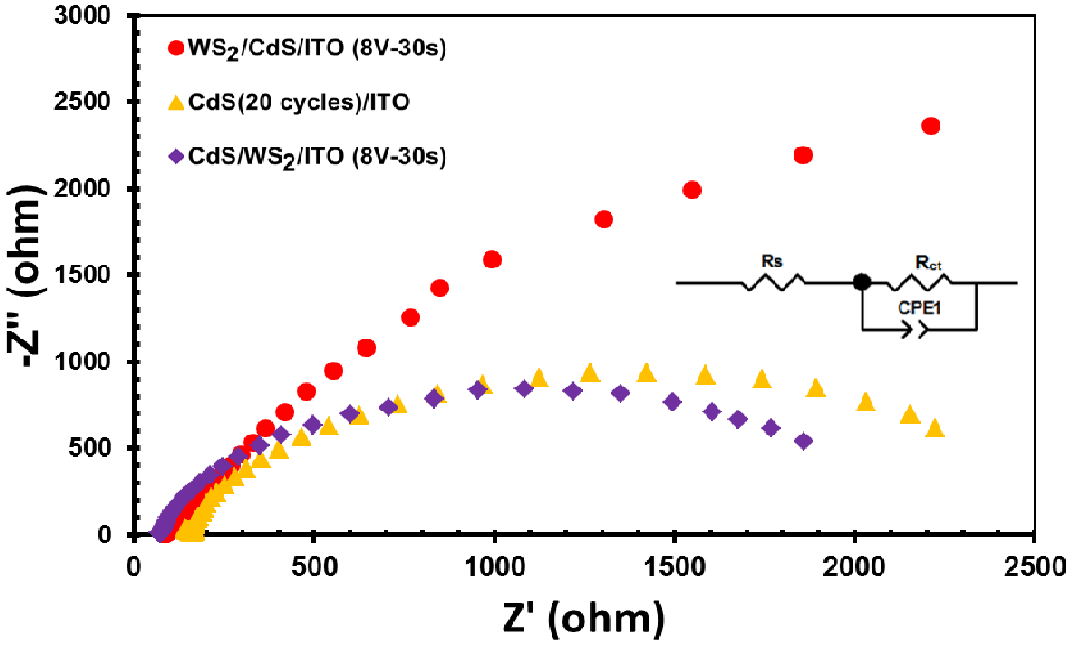
WS2/CdS/ITO (8V-30s)
CdS(20 cycles)/ITO
CdS/WS2/ITO (8V-30s)
Rs
Rct
CPE1
-Z'' (ohm)
Z' (ohm)
0
500
1000
1500
2000
2500
3000

Fig. 9

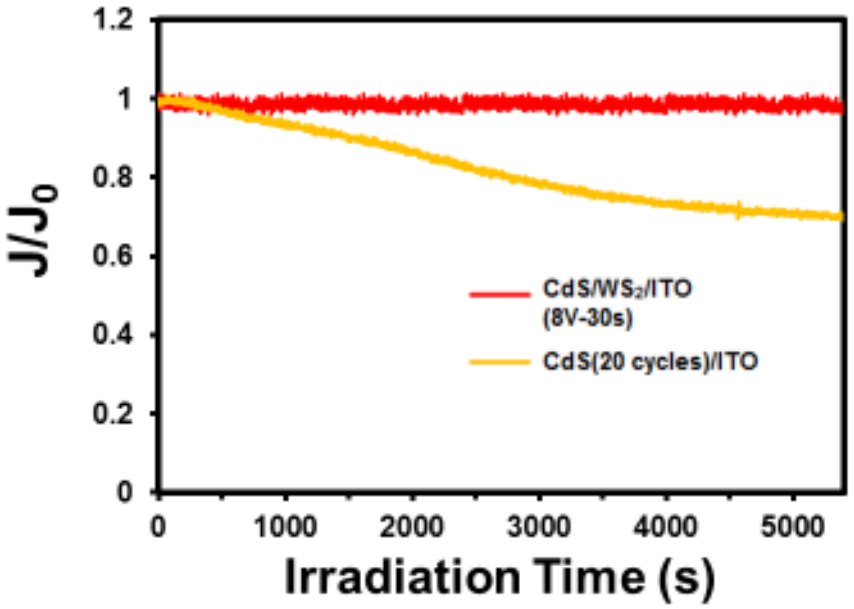
J/J0
Irradiation Time (s)
CdS/WS2/ITO
(8V-30s)
CdS(20 cycles)/ITO
0
0.2
0.4
0.6
0.8
1
1.2
0
1000
2000
3000
4000
5000

Fig. 10

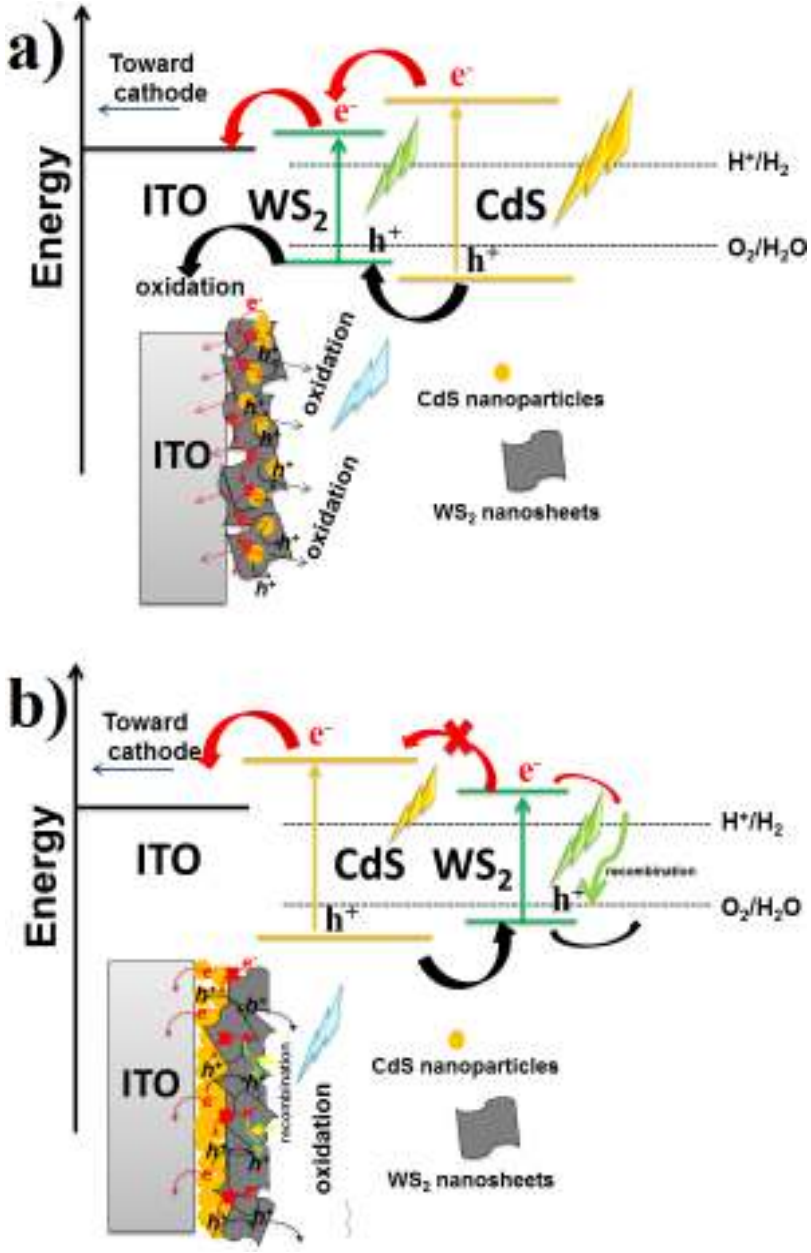
a)
Toward cathode
Energy
ITO
WS2
CdS
H+/H2
O2/H2O
oxidation
CdS nanoparticles
WS2 nanosheets
b)
Toward cathode
Energy
ITO
CdS
WS2
H+/H2
O2/H2O
recombination
oxidation
CdS nanoparticles
WS2 nanosheets